SIMULATION STUDY OF A NOVEL DIGITAL FOCUSED BEAMFORMER FOR DIRECTLY SAMPLED BANDPASS SIGNALS

J.G.Paul[1], R.McHugh[1] & G.A.Shippey[1]

[1] Heriot-Watt University, Ocean Systems Laboratory, Department of Electrical and Electronic Engineering, Edinburgh, EH1 2HT, Scotland.

1. INTRODUCTION

The technique to be studied is a digital focused beamformer for SONAR using directly sampled bandpass signals. The beamforming concept has been described in earlier papers [1,2]. Two distinct blocks exist; these are the data acquisition module and a digital processor for image construction. The output from each receiver array element is immediately amplified and directly sampled at a rate conforming to the Nyquist bandpass sampling criterion. The digitised data is stored in a space-time RAM. Image construction is based upon a priori knowledge of the sensor positions and focused spatial points of interest (in any coordinate system), this allows all possible time delay combinations to be pre-calculated and stored in a look-up table. This enables spatially distributed imaging in the near/far-field using any receiver array configuration.

A software simulation of the data acquisition and image construction modules of this sonar system has been developed. Preliminary results using this simulation were given in [1,2]. The simulation study presented examines the DSP processing and performance trade-offs involved in the technique. Specifically these are, the direct sampling ADC rate with narrow-band and wide-band signal processing; the density or distribution of the focused spatial points of interest; and the effects of typical DSP fixed-point storage restrictions. These results illustrate different operating conditions of the technique and provide an insight into the digital signal processing requirements of the overall focused beamforming system.

2. SONAR BEAMFORMER SYSTEM SIMULATION

2.1 Introduction

Simulation is a well established and important tool allowing system designers to understand complex systems and their behaviour. The rationale for computer simulation and analysis is diverse. It demands system abstraction, and therefore enables the general study and experimentation with the system parameters and their interactions.
The simulation that was developed, called IRIS (Image Realization In Simulation), models a complete digital sonar system from the point of pulse transmission to the synthesis of a sonar image. It is functionally split into two parts. Initially aspects of synthetic data generation are discussed. This covers simulation from pulse transmission to data acquisition and is based on a typical sonar system model. The main function of IRIS is the image realization software. This is the digital focused beamformer introduced in section 2.3. The simulations were created with the general purpose of obtaining a greater understanding of the point spread function (PSF) of the actual beamforming process itself.

2.2 Data Acquisition Simulation

A general sonar system model such as the one proposed by Winder [3], illustrates the interactions between the acoustic channel, scenario and the sonar transmitter/receiver. The general term sonar receiver also represents the beamformer, this is discussed in section 2.3 .

Acoustic Channel Modelling. Aspects of propagation modelling only were considered. The two main issues were the

frequency dependant attenuation losses and the spherical spreading losses with distance. IRIS assumes a direct acoustic ray path from the transmitter to reflector and back to the receiver, no multi-path signals are modelled.

Scenario Representation. IRIS uses a target model similar to the one put forward by Van Trees [4]. There are several alterations, such as arbitrary incident pulse envelopes, the target physical structure is composed of a single reflector, although several can be grouped together to represent a multiple point reflector. Finally, Doppler is not considered. White Gaussian noise is added to each receiver. This has negligible noise correlation between sensors. The received pulse r(t) can be written as,

$$r(t) = b(t)f(t-\tau)e^{j\omega_c t} + n(t)$$

b(t) is the pulse envelope function, f(t - τ) is a delayed replica of the transmitted pulse, $\omega_c=2\pi f_c$, f_c is the carrier frequency, and n(t) is ambient white Gaussian noise.

Sonar transmitter/receiver. The transmitter and receiver constitute the analogue and array front-end. Aspects that are modelled include arbitrary PCW or Chirp transmission and reception at arbitrary array transducer locations, anti-aliasing filtering, a stepped time-varied gain unit, analogue to digital conversion (ADC) and pulse compression filtering. ADC sampling rates and amplitude quantization effects are discussed later (sections 3.3,3.4 & 6.2 respectively).

2.3 Image Construction Simulation

Simulation of the image construction module in IRIS is implemented using a basic framework. This framework consists of a Pixel Coordinate Map (PCM) and a Look-Up Table (LUT). These definitions lead to the use of synthetic (or real) data in the beamformer algorithm to synthesise an image.

Pixel Coordinate Map Definition. In a static beamforming scenario, a single 2D matrix of focused spatial points needs to be defined. The coordinates of these points are stored in the PCM. The PCM is defined by knowing that the spatial window of interest is Xm by Ym centred at (x,y), and the final pixel image is size NxM. Thus each pixel has a one-to-one correspondence with a focused spatial point (see [2]), and therefore has a coordinate (stored as a polar ie. r,θ value). Quantization of the PCM is discussed in section 6.4.

Look-Up Table Definition. For faster execution during beamforming, IRIS stores the integer sample number in space-time RAM and the fractional phase shift necessary to focus precisely at every spatial point from every sensor. This requires knowledge of the pixel coordinates (defined above), the position of each sensor and the particulars of the ADC sampling scheme used. Using LUT based processing, imaging using a circular array is straight-forward, see section 3.5. Section 6.3 examines LUT quantization.

Algorithm Processing. The LUT and a data set (real or synthetic) are used to achieve image synthesis in the focused beamformer. IRIS processes the sensor data sequentially, sensor by sensor. Ideally this would be done in parallel. Sensor data is read in and apodized. The data is then processed according to the algorithm outlined in [1]. The image is built up pixel by pixel.

Final Image Display. Pixel magnitudes in the final image are normalised relative to the highest value within the image itself. Typical image dynamic ranges can be linear, 30dB or 200dB. Two formats for image display are used throughout the simulation results (to follow). Full 2D sonar images and 1D polar cuts are used. Polar cuts are radial plots of the point spread function (PSF) taken at a constant distance from the array centre over a 180° sector. The 2D images represent direct Cartesian coordinate representations of the spatial area of interest.

Processing Requirements. The total number of multiply operations required to generate a single image using this technique is based on the following key parameters. These are for a PxP (P^2) pixel image, T transducer array, S samples/transducer, C components in pulse model, B samples/local spectral estimate. S is dependant on the size of the spatial area of interest and the sampling frequency f_s. For an area spanning 100m in range and with f_s=44.444kHz, S = 667xB. B will be considered to be equal to the pulse length.

Two processing cases can be considered. Case i.) where $P^2 > S$ and case ii.) where $P^2 <= S$. Case i.) is where all the sensor data is immediately convolved with a spectral estimator on-line and requires,

$$2C[BST + P^2(2T+1)] \qquad (2.1)$$

MOPS (Multiply OPerations/Second). Case ii.) is where the section of sensor data to be convolved is specifically selected depending on the spatial point/pixel of interest, ie. the processing is pixel driven, therefore,

$$2CP^2(BT+2T+1) \qquad (2.2)$$

MOPS are required. These two equations will be used throughout the remainder of this paper. Figures 1a,b (0<BL<30 expanded) illustrate the relationship between B (proportional to the ADC sampling rate, f_s) and the number of MOPS (Multiply OPerations/Second). The two lines represent the two possible processing schemes in cases i.) and ii.) .

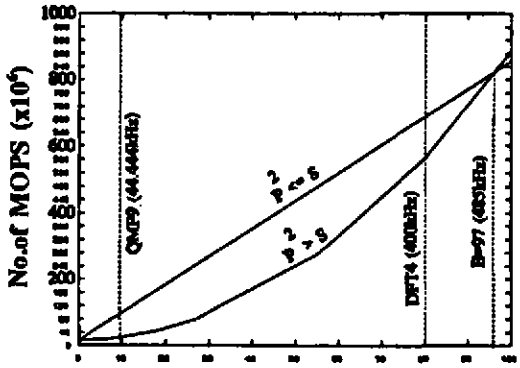

Block Length (20λ pulse length)
Figure 1a No. of MOPS v. BL

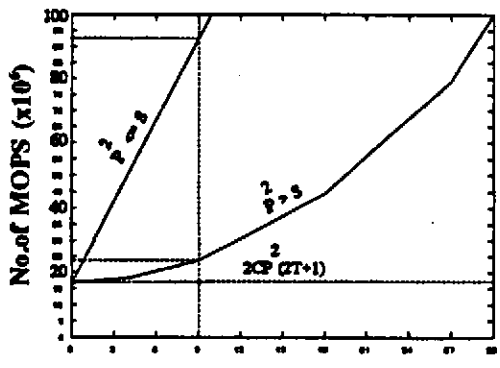

Block Length (20λ pulse length)
Figure 1b No of MOPS v. BL

3. BANDPASS SIGNAL FOCUSED BEAMFORMING

3.1 Introduction

One of the main considerations when using this technique is the sampling rate of the ADC. The sampling rate, f_s (assuming a specific pulse length) will determine the value of B in (2.1) . Narrow-band signal beamforming will restrict the value of C to 1, wideband signals use C>1.Initially, the selection of an appropriate sampling frequency below that of the carrier by directly sampling the signal will be considered. Both cases of narrow-band and wide-band performance will be considered in terms of the processing requirements using (2.1) & (2.2). The low sampling rate algorithm uses a Quadrature Matched Filter (QMF) spectral estimator on the sensor data to calculate the real and imaginary components, whereas, the high sampling rate spectral estimator is based on a DFT (narrowband) or FFT

(wideband), alternatives to the latter have been proposed [5].

3.2 First-order Sampling

This sampling technique is an alternative to conventional quadrature sampling methods [5]. Quadrature sampling requires two quadrature analogue mixers and suitable lowpass filters followed by two ADC's. First-order sampling is also known as direct sampling, and as the title implies, it directly digitises the incoming data and does not involve any form of analogue pre-processing apart from the usual amplification and anti-alias filtering. Direct sampling can only use specific sampling rates (f_s) depending on the carrier (f_c) and signal bandwidth Ω. These can be expressed as in eqn (3.1) below,

$$\frac{2}{n}.(f_c+\Omega/2) \le f_s \le \frac{2}{(n-1)}.(f_c-\Omega/2) \qquad (3.1)$$

Using (3.1) the following parameters are valid, f_c = 100kHz, Ω = 22.2kHz and f_s = 44.44kHz. This is an optimal sampling frequency as it is twice the bandwidth, and can only be achieved for specific f_c:Ω ratios.

3.3 Narrow-Band Signal Study

The results shown in Figures 2 & 3 illustrate the radial point spread function of a point at 60m from the array and 10° from broadside. These polar cuts consist of 1441 focused points on the radius over 180°, therefore each focused spatial point is separated by 1/8°. A Rectangular envelope comprising of 20λ's was transmitted at 100kHz (pulse length = 0.3m). The array consists of 64 linearly arranged transducers, separated by λ/2. The ADC digitises to 8 bits.

In Figure 2, the QMF based algorithm with a sampling rate of 44.444kHz is used, the PSF plots are displayed as polar cuts in order to appreciate the shape of the PSF. (a.) is with 0dB sensor data noise using a 40dB stopband attenuation on the anti-aliasing filters, (b.) is in the same noise conditions with a 119dB stopband attenuation, while (c.) is the radial PSF with a SNR of 97dB. (c.) shows a typical rectangularly apodized diffraction pattern around the main lobe. The fact that the pulse does not propagate across the whole array at the same time cause the pattern to degenerate to an average image noise level (INL) of -45dB. (b.) illustrates the advantage of using a high stopband attenuation for anti-aliasing (INL = -36dB), as opposed to (a.), (INL=-15dB). Therefore, the imaging performance markedly degrades as the stopband attenuation decreases.

Figure 3 uses f_s = 400kHz and the DFT based algorithm. (a.) avoids aliasing but does not prefilter the 0dB sensor data signal, (b) has 97dB sensor data noise. (a.) produces a -37dB INL which is the same as Figure 2 (b.), illustrating the fact that the lower sampling rate could give comparable imaging performance in noise conditions by treating the antialiasing filter as a noise rejection stage.

Although the PSF's shown were 1 dimensional (radial only), the processing requirements for a 2D PSF comprising of 256x256 pixels in the image can be calculated based on equations (2.1) or (2.2). To obtain a 256x256 image using f_s = 44.444kHz. implies that B=9, and from Figures 1a & 1b this leads to a processing requirement of 23.82x10^{6}MOPS. With f_s = 400kHz. (B=80) requires 563.32x10^{6}MOPS. Note that both calculations are taken from the $P^2 > S$ line (the most efficient processing scheme in this situation).

3.4 Wide-Band Signal Study

Figure 4 illustrates the radial PSF of the same point discussed above. A Rectangular envelope comprising of a Chirp source of bandwidth 40kHz centred at 100kHz was transmitted. 0dB sensor data noise was included. Again, the array consisted of 64 linearly arranged transducers, separated by λ/2, however, λ was based on a frequency of 130kHz. The ADC also digitised to 8 bits using a sampling rate of 133.333kHz . f_s is sub-Nyquist (lowpass

criterion=>240kHz or more), and ensures no aliased spectral overlap for signals with a bandwidth less than 66.667kHz. All the PSF plots use a DFT/FFT with a predesigned time domain window to reduce spectral leakage.

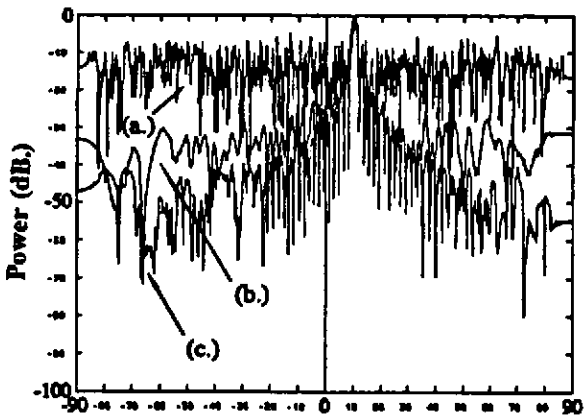

Figure 2 QMF based algorithm

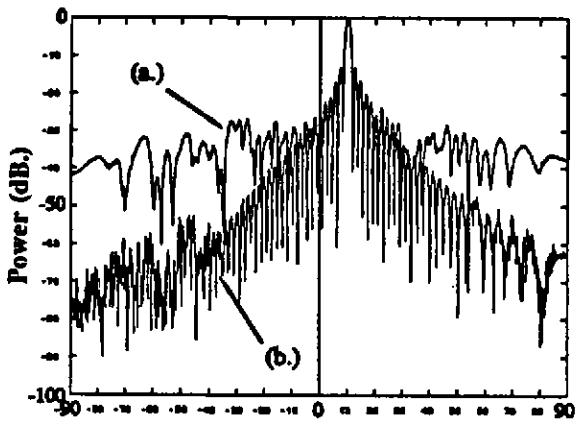

Figure 3 DFT based algorithm

Only one component is used in (a.). When the number of components used in the beamforming algorithm is increased to 7 (b.) or even 19 (c.) the image noise level tends to smooth itself out, but the diffraction pattern remains the same around the mainlobe.

The processing requirements for a 2D PSF comprising of 256x256 pixels using f_s = 133.333kHz. implies that B=64, (S=18000 for 100m coverage) and from equation (2.1) this leads to a processing requirement of 164.36×10^6MOPS for a single component. The $P^2 > S$ line is used. For 7 components, this increases by a factor of 14, and for 19 components, by a factor of 38. Obviously, the number of spectral components used is a crucial factor in the processing requirements. Work on reducing the number of components required, is pursued in [5].

3.5 Circular Array Processing

Briefly, Figure 5 below shows two superimposed radial PSF's of three points at 60m at 0°,35° and 75° from broadside. The array used was a $\lambda/2$ spaced circular array. The array diameter was the same as the 64 element narrowband array used in section 3.2, therefore, the complete circumference comprised of 198 elements, $\pi(64-1)$. The result shows, as expected, a consistent mainlobe width as the angle of incidence moves towards endfire (no mainlobe broadening, cf. linear array), and 8dB sidelobes, consistent with the Bessel function type diffraction pattern. This example could have illustrated the beamformer with any array element distribution (ie. conformal, random) and shows the advantages of a LUT based processing scheme. The amount of processing is slightly less than that of a 198 element linear array, because not all array elements are visible to all the focused spatial points on the 60m radial arc.

4. FOCUSED SPATIAL POINT DISTRIBUTION

4.1 Introduction

Focused beamforming that is based on processing for each pixel/spatial point of interest is affected by the total number of pixels, P^2, in the final image. In turn, the density of the distribution of the focused spatial points within the area of interest is also affected by the size of the area. By simply applying the 2D sampling theorem, one can obtain a valuable insight into the required density of focused points within a pre-defined area such that the point

spread function is adequately sampled in space. There is then the important trade off between the image quality and

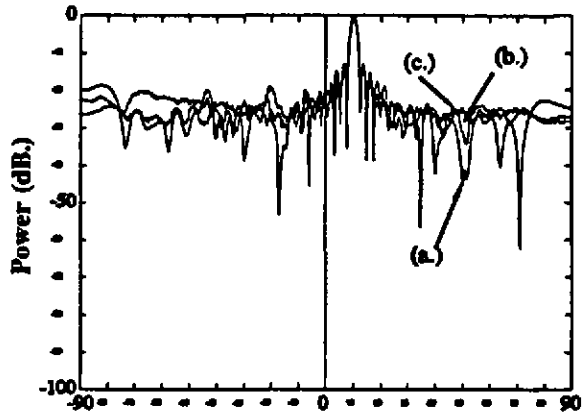

Figure 4 Wideband signal beamforming

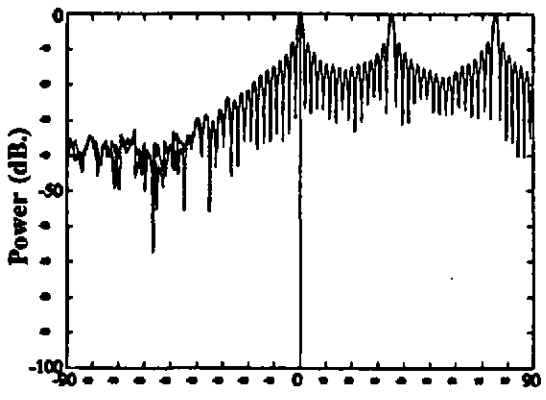

Figure 5 Circular array beamforming

the processing. It is important to note that in general search situations over large areas of interest, the image quality may not be of primary importance, whereas in detailed close up situations the ability to zoom by increasing the density of the spatial points is vitally important. The following images illustrate the trade-off between image quality due to the spatial point distribution/density and the processing requirements.

4.2 Spatial Point Distribution Study

A 20λ, 100kHz Gaussian pulse was used for this study. The process of selecting appropriate lateral and longitudinal spatial sampling intervals depends on the location of the spacially variant PSF within the spatial window (area of interest). For example, using a 64 element, λ/2 spaced array and the QMF (f_s=44.444kHz) based beamforming algorithm with a point at (30m,+35°), the PSF produced by the imaging system can be analyzed. A 2D FFT of the PSF (in Cartesian coords) reveals a maximum row and column frequency that can be related to minimum lateral (δ_{lat}) and longitudinal (δ_{long}) sampling intervals in metres. These were calculated to be 0.133m and 0.136m respectively. For convenience 0.135m will be used for both.

Figure 6 below shows a 2D synthesised sonar image of a 76.5m^2 spatial window comprising of 256x256 focused spatial points or pixels. Therefore, $\delta_{lat}=\delta_{long}$=0.3m, which is 2.22 times the required minimum spatial sampling rate (δ_{min}). As can be seen, the clusters of points at (60m,0°), (30m,+35°) and (5m,-75°) are not discernable at all. In terms of the processing requirements, the number of pixels P^2 in the image, C (=1) and T (=64), define the minimum MOPS for image synthesis (see Figure 1a). For Figure 6, P^2>S (S=6000 for 100m area), and 23.82x10^6 MOPS are required.

In operational situations where further detail is needed, selected areas could be zoomed into. The area marked 'A' in Figure 6 is an inadequate representation of the 6m^2 area. It is spatially sampled at 16x16 focused points/pixels in Figure 7 where $\delta_{lat}=\delta_{long}$=0.4m = 2.96$\delta_{min}$, therefore, a denser spatial point distribution is required. The number of MOPS is calculated using a value of S=600 due to the reduced 6m^2 area of interest. The P^2<S processing scheme is the best choice, and using (2.2), 0.361x10^6 MOPS are required.

32x32 spatial points are used in Figure 8, therefore $\delta_{lat}=\delta_{long}$=0.194m = 1.44$\delta_{min}$, but the cluster is still hard to discern. With P^2>S, 0.955x10^6 MOPS are required. Finally, Figure 9 samples the area with 128x128 spatial points/pixels,

resulting in $\delta_{lat}=\delta_{long}=0.0472m = 0.35\delta_{min}$. With this density of spatial points, the cluster is discernable.

The 0.35 figure represents the spatial sampling interval, relative to the minimum value calculated by the 2D FFT of the PSF. Therefore, a sampling interval of at least half δ_{min} is required cf. 2D analogy of 1D Nyquist sampling theorem. Figure 9 is synthesised with the $P^2>S$ scheme and requires $4.92x10^6$ MOPS.
Further examination of this figure shows pairs of points at increasing angular separations. The separations are 1.5,2.0,2.5,...,4.0 normal beamwidths at 30°. The figure reveals the beamformer resolution to be approx. 1.5 normal beamwidths with *coherent* (in-phase) point objects.

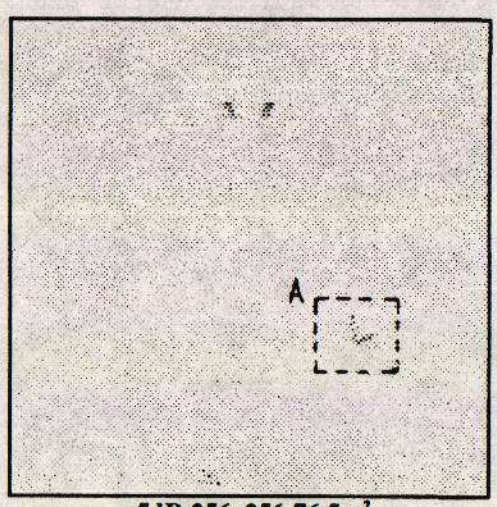

-5dB 256x256 76.5m²
Figure 6 $2.22\delta_{min}$

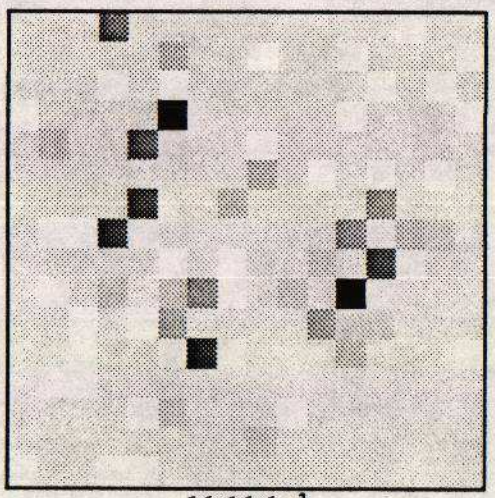

16x16 6m²
Figure 7 $2.96\delta_{min}$

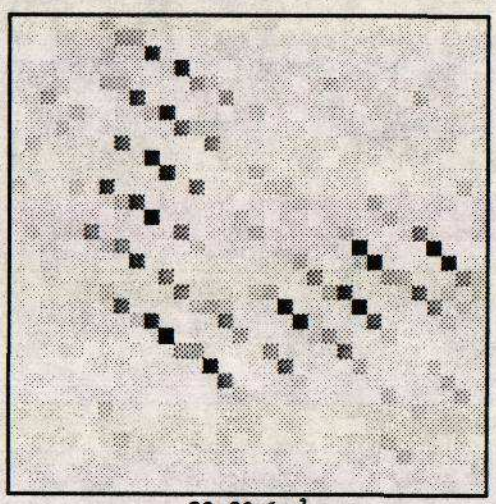

32x32 6m²
Figure 8 $1.44\delta_{min}$

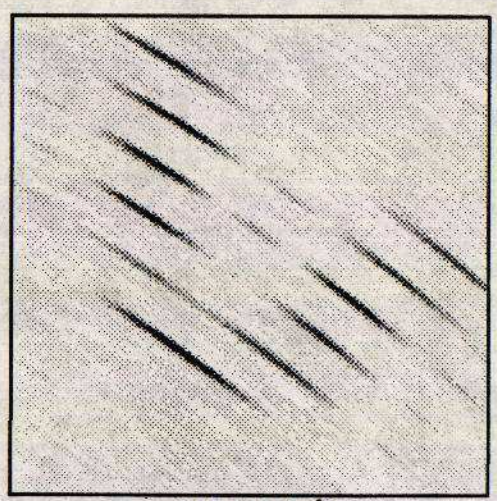

128x128 6m²
Figure 9 $0.35\delta_{min}$

6. FINITE BIT LENGTH EFFECTS

6.1 Introduction

In any real sonar system there are limitations in accuracy due to the finite bit lengths involved in storage. The following brief analysis will attempt to evaluate the significances of data bit sizes in the digital focused beamforming technique.

6.2 ADC Quantization Study

Section 3.1 considered the ADC sampling rate. Previous results use an 8 bit ADC. This section will consider the effects of the finite bit data representation due to ADC amplitude quantization. A 20λ Gaussian transmit pulse is used with the standard 64 element, λ/2 element spaced array. By using the QMF (f_s=44.444kHz) based algorithm, approximately the same diffraction pattern was obtained to within 1dB when using 8 or more bits. The signal being sampled used the complete dynamic range of the ADC. Differences were apparent when less than 8 bits were used. Figure 10 compares images where 8 bit and 2 bit ADC's were used. Obviously, the increased quantization noise in the data due to the ADC amplitude quantization has raised the image noise level from (a.) 8 bit = -55dB to (b.) 2 bit = -28dB.

Figure 11 uses the single component DFT based algorithm using f_s=400kHz. (a.) uses an 8 bit ADC while (b.) uses a 2 bit ADC. (a.) has a image noise level around -70dB, which is representative of the ADC noise alone. Also noticeable is a -55dB quantization lobe at -45° due to the discrete time sampling nature of the ADC. In (b.) the noise level has increased to -35dB. This noise level is lower than that in Figure 10 (a.). One noticeable feature is that the minimum noise level using the higher sampling rate is due to the ADC quantization noise, whereas at the lower sampling rate this is not the case and the likely cause is the low f_s at the ADC.

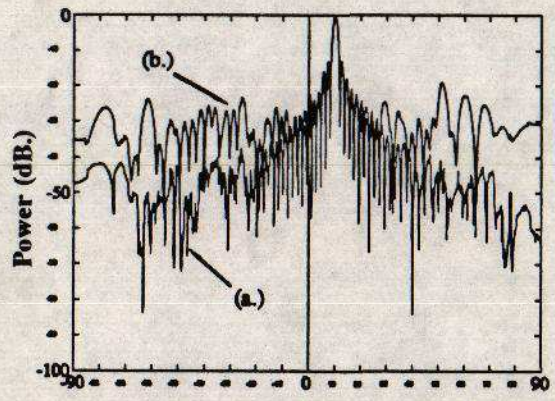

Angle from broadside (°)
Figure 10 (QMF) 8bit & 2bit ADC

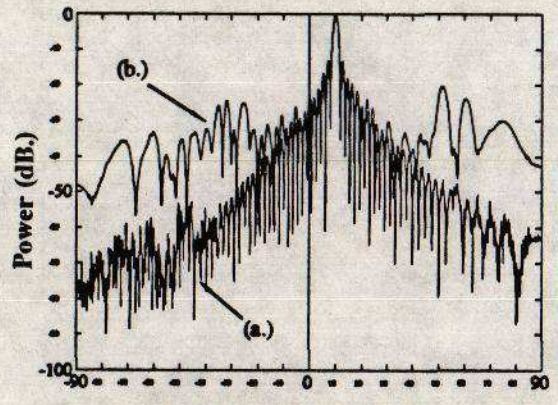

Angle from broadside (°)
Figure 11 (DFT) 8bit & 2bit ADC

6.3 LUT Quantization Study

A key feature of this focused beamformer is the ability to fine phase shift between data samples in space-time RAM. This relies on the bit size and accuracy of the LUT (section 2.3) used to select the appropriate data. Conventional time domain beamformers use the data samples as they are (up-sampled or not) and typically exhibit what are called quantization lobes [6]. These beamformers can be approximately simulated by using a LUT with zero bits in the fractional part, ie. only integer delays are used. This is compared with 12 bit fractional LUT quantization for both f_s=44.444kHz (Figure 12) and f_s=400kHz (Figure 13). Figure 12 (a.) shows the typical QMF radial PSF, but with zero bits LUT quantization (integer delays only). In (b.) beamforming is not possible due to the low sampling rate. Figure

13 (a.) uses the DFT single component spectral estimator and exhibits the afore-mentioned 8 bit ADC noise level with a quantization lobe at 50°. (b.) illustrates the conventional time domain beamformer performance where there is a average time quantization noise level of -35° and a much higher quantization lobe (-20dB as opposed to -53dB). The necessity of fine phase shifting is obvious with f_s=44.444kHz, while it provides a much improved beamformer performance with f_s=400kHz.

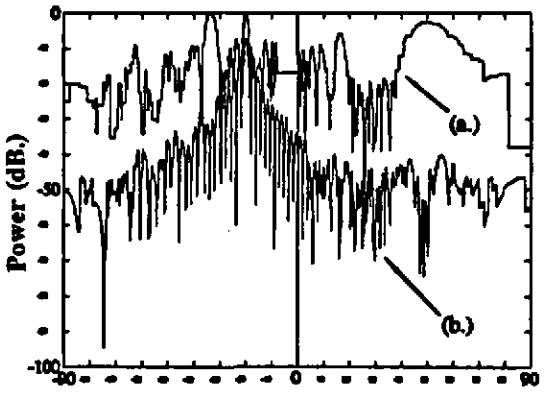

Angle from broadside (°)
Figure 12 (QMF) 12bit & 0bit LUT

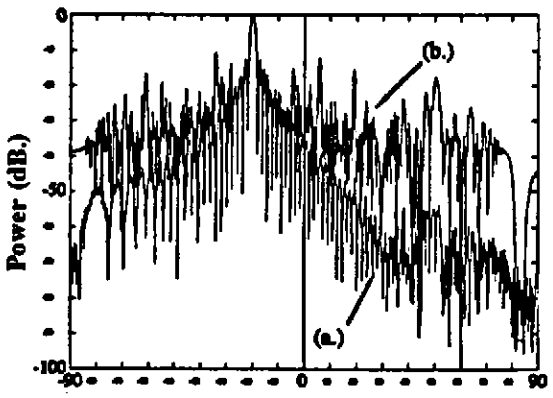

Angle from broadside (°)
Figure 13 (DFT) 8bit & 0bit LUT

6.4 Coordinate Quantization Study

Quantization of the Pixel Coordinate Map (PCM, section 2.3) is effectively the same as uniformly distributed position errors (stabilization errors) in the focused spatial points (distributed as discussed in section 5). The PCM consists of (r,θ) coordinates of all these points and the amount of quantization in each of these parameters necessary to provide a reasonable image quality will be presented. A cluster of twelve points around (5m,-75°) from the 64 element, λ/2 array, using a 20λ Gaussian pulse will be used with the QMF based algorithm.

Figure 14 shows the cluster using 8 bit θ quantisation, and 30 bit r quantization (negligible). This is equivalent to +/-0.11° angular error, 6 bit θ quantization (not shown) produced a bad image (equivalent angular error = +/-0.45°). Figure 15 is of the same cluster but using 8 bit r quantization, with negligible (30 bit) θ quantization. The radial (r) error is +/-1.95mm (= 0.13λ). With 6 bit r quantization (not shown) the intolerable image was equivalent to a radial error of +/-7.81mm (= 0.52λ).

Note that PCM quantization has been examined for different point positions and is found to be spacially variant. Radial quantization is less significant at wider angles from broadside, whereas angular quantization becomes more significant.

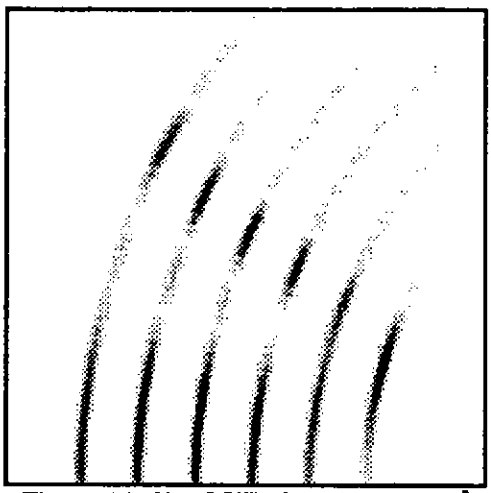

Figure 14 8bit LUT (θ), 256x256, 6m²

Figure 15 8bit LUT (r), 256x256, 6m²

The work was jointly funded by the Marine Technology Directorate Ltd, (MTD), agents of the Science and Engineering Research Council, (SERC), BP Petroleum Development Ltd., Shell UK Exploration & Production, Department of Energy - Offshore Supplies Office, Ministry of Defence - Admiralty Research Establishment (now Defence Research Agency - Maritime Division), Alliant TechSystems Inc., Slingsby Eng. Ltd., Simrad Ltd.
The work is continuing under funding from the Marine Technology Directorate Ltd. (SERC agents) and Defence Research Agency - Maritime Division.

7. REFERENCES

[1] G.A.SHIPPEY, R.McHUGH & J.G.PAUL, 'Digital Holographic Imaging for Underwater Acoustic Applications', 19th Int. Symp. on Acoustical Imaging, Ruhr-University, Bochum, Germany, April 3-5, 1991.
[2] R.McHUGH, G.A.SHIPPEY & J.G.PAUL, 'Digital Holographic Sonar Imaging', IEE Institute of Acoustics, Int. Conf., Keele University, UK, April 15-19, 1991.
[3] A.A.WINDER, 'Sonar System Technology', IEEE Trans Sonics & Ultrasonics, Vol. 22, No. 5, pp291-332, Sept. 1975.
[4] H.L.VAN TREES, 'Detection, Estimation, and Modulation Theory - Part III', John Wiley & Sons, New York, 1971.
[5] G.A.SHIPPEY, R.McHUGH & J.G.PAUL, unconfirmed title, Ibid.
[6] D.K.PETERSON & G.S.KINO, 'Real-Time Digital Image Reconstruction: A Description of Imaging Hardware and an Analysis of Quantization Errors', IEEE Trans Sonics & Ultrasonics, Vol. 31, No. 4, pp337-351, July 1984.